nature photonics

Article

https://doi.org/10.1038/s41566-025-01651-y

Generation of ultrafast magnetic steps for coherent control

Received: 9 August 2024

Accepted: 26 February 2025

Published online: 2 April 2025

Check for updates

G. De Vecchi[1,4], G. Jotzu[1,4] ✉, M. Buzzi[1,4] ✉, S. Fava[1,4], T. Gebert[1], M. Fechner[1], A. V. Kimel[2] & A. Cavalleri[1,3] ✉

A long-standing challenge in ultrafast magnetism and functional materials research, in general, has been the generation of a universal, ultrafast stimulus able to switch between stable magnetic states. Solving this problem would open up many new opportunities for fundamental studies, potentially impacting future data storage technologies. Ideally, step-like magnetic field transients with infinitely fast rise time would serve this purpose. Here we develop a new approach to generate ultrafast magnetic field steps by quenching supercurrents in a superconductor. We achieve magnetic field steps with millitesla amplitude, picosecond rise times and slew rates approaching 1 GT s^{-1}. We test the potential of this technique by coherently rotating the magnetization in a ferrimagnet. Although in the current geometry, the magnetic field step is not sufficient to achieve complete switching, suitable improvements in the device geometry could make these magnetic steps both larger and faster. We foresee new applications ranging from quenches across phase transitions to complete switching of magnetic order parameters.

Ultrafast magnetic field steps are unipolar, time-varying magnetic field pulses with short rise times and long decay times, which are promising as a universal means to control magnetization[1–6]. Microcoils have been used to generate magnetic field steps with amplitudes of tens of milliteslas and rise times of hundreds of picoseconds or longer[7–9]. Auston switches can generate faster steps and are used to produce magnetic pulses with picosecond rise times and sub-nanosecond decay times[10,11]. In this case, the amplitude of the generated magnetic field is limited by Joule heating in the resistive coplanar waveguides carrying the pulse. Moreover, the spatial profile of the generated magnetic field is generally confined to micrometre-sized regions (tens of micrometres) with strong spatial gradients. Alternatively, picosecond magnetic field pulses with Tesla-level amplitudes are generated with relativistic electron bunches[12,13].

Intense ultrafast magnetic transients have also been produced starting from circularly polarized light pulses. In materials with a large Verdet constant, the inverse Faraday effect generates a transient magnetic field induction that follows the envelope of the driving pulse[14–17]. Similarly, circularly polarized terahertz and mid-infrared pulses can excite circular phonons, where the atomic motions generate effective magnetic fields as high as ~36 mT (ref. 18) and ~20 mT (ref. 19), a value four orders of magnitude larger than the theoretically predicted value[20]. Despite the importance of these findings, the nature of these magnetic transients remains poorly understood. It is particularly unclear whether these are analogous to conventional fields governed by Maxwell's equations or synthetic fields confined to the material, unable to propagate outside the sample[21].

Here we present a new tabletop method to overcome many of these shortcomings and demonstrate the generation of magnetic field steps that retain the fastest rise times, long decay times and sizeable amplitudes, and offer new opportunities for tailoring the spatial and temporal profiles of the induced magnetic fields.

The physical principle that enables the generation of magnetic steps with picosecond rise times and 'on' times far over a nanosecond (and potentially as long as milliseconds) is based on a superconducting material with large diamagnetism, quenched with an ultrafast optical

[1]Max Planck Institute for the Structure and Dynamics of Matter, Hamburg, Germany. [2]Radboud University, Institute for Molecules and Materials, Nijmegen, The Netherlands. [3]Department of Physics, Clarendon Laboratory, University of Oxford, Oxford, UK. [4]These authors contributed equally: G. De Vecchi, G. Jotzu, M. Buzzi, S. Fava. ✉e-mail: gregor.jotzu@mpsd.mpg.de; michele.buzzi@mpsd.mpg.de; andrea.cavalleri@mpsd.mpg.de

https://doi.org/10.1038/s41566-025-01651-y

pulse. Applying a magnetic field to a zero-field cooled superconductor generates persistent currents[22,23] to exclude the magnetic flux from the sample volume. We use sub-picosecond high-frequency laser pulses to disrupt superconductivity[24–29], and prompt a sudden change in the magnetic field near the material. In this way, we generate near-field, ultrafast magnetic steps. These pulses are extremely broadband, with frequency content spanning several octaves, from sub-gigahertz to terahertz frequencies.

Here we used a thin film of optimally doped $YBa_2Cu_3O_7$, cooled below T_c and excited with a 100-fs-long, 400-nm-wavelength optical pulse, which disrupts superconductivity[24–29]. To track the temperature and time evolution of the magnetic field surrounding the superconductor after optical excitation, we used a time-resolved magneto-optical imaging technique[30–32]. We placed a diamagnetic GaP(100) crystal above the superconductor, and the fast Faraday response to the local magnetic field was probed with a time-delayed optical pulse with 50-µm spatial resolution. Previous realizations of this field detection technique used ferrimagnetic detectors[33–35], limiting the time resolution to ~100 ps. Here we use diamagnetic GaP as a magneto-optic detector, allowing for a time resolution better than ~1 ps at the expense of a smaller signal and longer measurement times (Supplementary Section 1).

Thermally driven magnetic field step

A 1-mm-diameter disc with a well-defined edge was prepared using optical lithography, starting from a 150-nm-thick film of superconducting $YBa_2Cu_3O_7$ grown on Al_2O_3. We placed a 75-µm-thick (100)-oriented GaP crystal in close contact with the $YBa_2Cu_3O_7$ film (Supplementary Sections 2 and 3). The two formed a stack with the magneto-optic detector on top and the superconducting device right beneath it (Fig. 1a).

The $YBa_2Cu_3O_7$ sample and GaP detector were subjected to a 2-mT uniform magnetic field applied along the z direction using a Helmholtz coil pair (Fig. 1a). A linearly polarized 800-nm ultrashort probe pulse was focused to a spot size of ~50-µm full-width at half-maximum, impinging at near-normal incidence on a wedged GaP crystal. The Faraday effect induced a polarization rotation on the beam transmitted through the GaP and reflected from its second surface, yielding a measurement of the vertical component of the local magnetic field, averaged over the volume traversed by the probe in the magneto-optic detector. The external applied magnetic field H_{app} was sinusoidally modulated in time, synchronously to the laser probe pulse train. In this way, signals acquired with $-H_{app}$ were subtracted from those acquired with $+H_{app}$ (Supplementary Sections 4 and 5). This measurement protocol isolated contributions to the polarization rotation having a magnetic origin and suppressed potential non-magnetic contributions such as static and pump-induced birefringence.

Because H_{app} was varying in time as $YBa_2Cu_3O_7$ was held in its superconducting state, the magnetization in the superconductor originated from the exclusion of a time-varying magnetic field rather than the expulsion of a static magnetic field as in the Meissner effect. Compared with applying static magnetic fields, this protocol is advantageous because it minimizes the effect of trapped flux[22] and leads to the largest possible magnetic field steps (Supplementary Sections 6 and 7).

Figure 1a displays a finite-element simulation of the z component of the magnetic field surrounding the sample. We simulate the magnetic field exclusion in $YBa_2Cu_3O_7$ by modelling it as a medium with virtually infinite conductivity and applying a time-dependent external magnetic field (Supplementary Section 7). The magnetic field is reduced above the sample (blue regions) and increased near its edges (red regions) as the magnetic flux is kept from the sample.

Figure 1b (left inset) shows a two-dimensional map of the z component of the magnetic field measured when the $YBa_2Cu_3O_7$ disc is cooled to $T = 30\ K < T_c$. As predicted from the simulations, we observed a reduction in the local magnetic field when measuring above the disc (blue area) and a corresponding enhancement near the edge (red area).

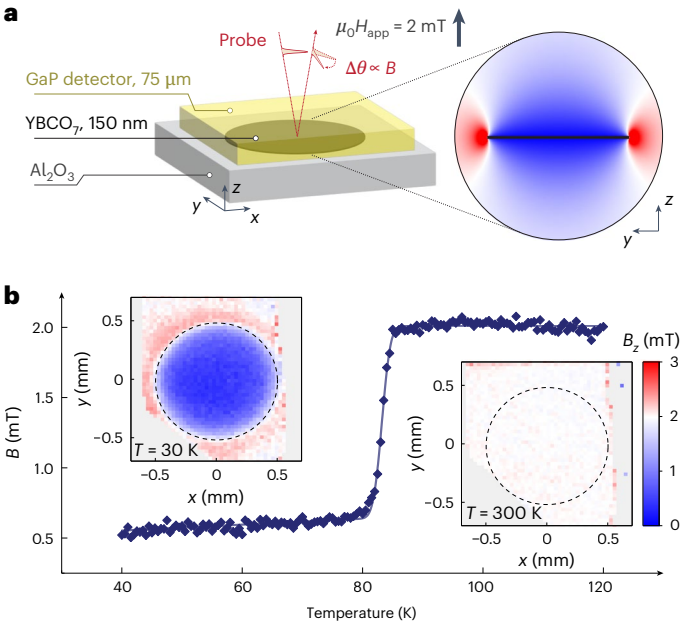

Fig. 1 | Thermally driven magnetic field step. a, Sketch of the experimental geometry. A 150-nm-thick, 1-mm-diameter $YBa_2Cu_3O_7$ ($YBCO_7$) disc was grown on an Al_2O_3 substrate. The local magnetic field surrounding the $YBa_2Cu_3O_7$ disc is measured by tracking the Faraday polarization rotation of a linearly polarized 800-nm probe pulse, reflected after propagation through a 75-µm-thick GaP(100) crystal placed on top of the sample. A 2-mT magnetic field (B_{app}) is applied in the z direction. Its polarity is periodically cycled to isolate the magnetic contributions to the polarization rotation. The colour plot (zoomed-in view) illustrates the simulated (Supplementary Section 7) changes in the z component of the local magnetic field (B_z) induced by the superconductor below T_c. Blue (red) indicates areas with reduced (enhanced) magnetic field, following the colour scale shown in **b**. **b**, Temperature dependence of B_z measured above the centre of the $YBa_2Cu_3O_7$ disc. Each data point represents the mean value ± s.e.m. (smaller than the size of the data points) extracted from a sample of 100 acquisitions (Supplementary Section 5). A clear transition at $T_c = 85$ K is observed. The measured field exclusion is not complete due to the finite thickness of the GaP detector, which leads to averaging in the z direction (see the main text and Supplementary Section 8). The left inset shows a two-dimensional map of B_z, measured as a function of the x and y positions at $T = 30\ K < T_c$. An increase in the magnetic field is measured near the sample edge (red), and a reduction above its centre (blue). The dashed black line indicates the outline of the superconducting disc. The right inset shows the same measurement at $T = 300\ K > T_c$. No spatial dependence is observed throughout the field of view.

The amplitude of the measured changes is determined by the geometry of the experiment and by the thickness of the detection crystal (Supplementary Section 8). The same measurement was repeated at $T = 300\ K > T_c$. The results are displayed in Fig. 1b (right inset), showing that when the $YBa_2Cu_3O_7$ disc is in its normal state, no spatial dependence of the local magnetic field is detected.

The temperature was then varied between 40 K and 120 K to track the evolution of the magnetic field above the centre of the $YBa_2Cu_3O_7$ disc (Fig. 1b). As the temperature was swept across $T_c \approx 85$ K, a sharp change in the magnetic field was observed, resembling a magnetic field step. The speed at which this magnetic field change can be induced by varying the temperature is limited by how fast the material is heated or cooled through the transition (~0.3 K s^{-1}), limiting the highest frequency content to less than a few hertz.

Ultrafast magnetic field step

Picosecond rise times were achieved by irradiating $YBa_2Cu_3O_7$ with ultrashort optical pulses, which disrupt superconductivity depleting the condensate on ultrafast timescales[24–29] (Supplementary Section 9 provides a more in-depth review on the disruption mechanisms). After

https://doi.org/10.1038/s41566-025-01651-y

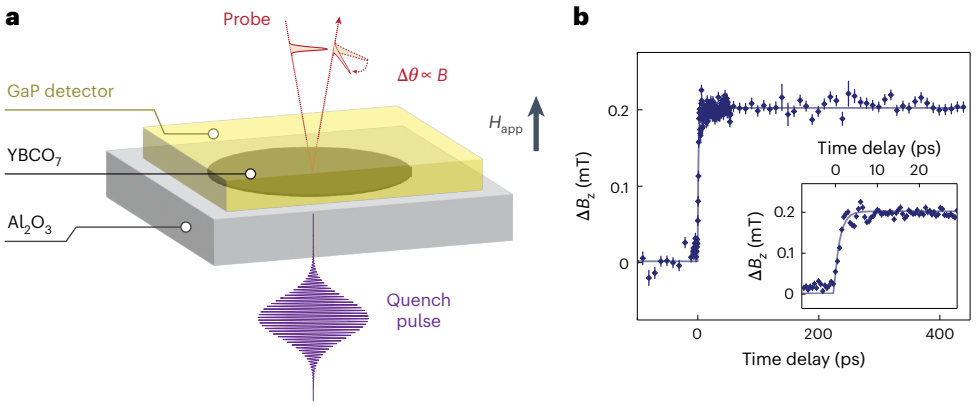

Fig. 2 | Ultrafast magnetic field step. a, Sketch of the experimental geometry. The sample–detector assembly is the same as that in Fig. 1a. The $YBa_2Cu_3O_7$ disc is kept at a base temperature $T = 55\ K < T_c$ and photoexcited with an ultraviolet laser pulse ($\lambda = 400$ nm) to disrupt superconductivity. This quench pulse is shaped into a flat-top disc by a shadow mask and imaged by a 4*f* imaging system onto the $YBa_2Cu_3O_7$ disc (Supplementary Section 11). The pump-induced changes in the local magnetic field were quantified using Faraday magnetometry in a GaP(100) detector as a function of the time delay between the probe and quench pulses. A 2-mT magnetic field (B_{app}) is applied in the *z* direction. Its polarity is periodically cycled to isolate the magnetic contributions to the polarization rotation. **b**, Quench-induced changes in the *z* component of the local magnetic field ΔB_z, measured above the centre of the disc as a function of the pump–probe delay. Each data point represents the mean value ± s.e.m. extracted from a sample of 1,100 acquisitions (Supplementary Section 5), and the solid line is a fit with a single-time-constant exponential model (Supplementary Section 10). The inset shows a zoomed-in view at short time delays around time zero. The value of the measured magnetic field at negative time delays is equal to 0.45 mT due to the dynamics of the trapped flux in the superconductor between consecutive pump pulses (Supplementary Section 14).

disruption, we expect the supercurrents shielding the applied magnetic field to disappear on a timescale probably determined by the L/R time constant of the resistive disc (L is the total inductance of the disc and R is the resistance in the photoexcited state). As a result, we expect the magnetic field to penetrate back into the sample volume on the same timescales (Supplementary Section 10).

The geometry of the experiment (Fig. 2a) was the same as that used in the temperature-dependent measurements, with the only addition of a quench pulse (centre wavelength, 400 nm; duration, ~100 fs; fluence, ~0.3 mJ cm^{-2}), which struck the sample from the side opposite to the GaP detector. Note that the $YBa_2Cu_3O_7$ thin film was opaque to 400-nm radiation, and the quench beam was shaped like a disc with a flat intensity profile imaged onto the sample to match its size (Supplementary Section 11). These precautions prevented a direct interaction of the ultraviolet pump with the magneto-optic detector that could give rise to nonlinear interactions leading to spurious responses (Supplementary Section 12 shows that no magnetic pump–probe signal was detected when the device was kept at 100 K, above T_c of the superconductor). Furthermore, the measurements were performed using the differential magnetic field scheme described above, isolating signals only connected to the applied magnetic field H_{app}.

Figure 2b displays the time dependence of the changes in the local magnetic field induced by the quench pulse and measured above the centre of the $YBa_2Cu_3O_7$ film at a base temperature $T = 55\ K < T_c$. As shown in Fig. 1b, the $YBa_2Cu_3O_7$ shields the applied magnetic field effectively at this temperature. As the quench pulse hit the sample, an increase in the magnetic field was detected. This change produced an ultrafast magnetic field step of ~0.2-mT amplitude with a rise time of ~1 ps (Fig. 2b, inset), corresponding to a slew rate of ~200 MT s^{-1} (further details about this measurement and the fitting procedure are reported in Supplementary Sections 10, 12 and 13).

An equivalent L/R circuit describes the system's dynamics well when assuming a conductivity of the excited state of 0.1 MS m^{-1}, which is lower than, but comparable to, the normal-state conductivity of $YBa_2Cu_3O_7$ (refs. 36,37). The validity of this model is confirmed by finite-element simulations, which predict a time constant that scales linearly with the diameter of the disc (more details are described in Supplementary Section 10).

Importantly, after the transient, the magnetic field remained constant for several hundreds of picoseconds even if the superconductivity in $YBa_2Cu_3O_7$ thin films is expected to recover within a few picoseconds after photoexcitation[27] (Supplementary Section 9). That is the case since the superconductor's equilibrium and photoexcited magnetic responses originate entirely from shielding currents, screening the time-dependent applied magnetic field (Supplementary Sections 6 and 14). When the superconductor recovers after the quench in an applied magnetic field, only a weak Meissner expulsion appears, which gives rise to a response that is below our experimental field resolution (Supplementary Section 7). Note that in alternative realizations of magnetic field steps, based on Auston switches or by free-space terahertz pulses, the low-frequency cut-off is generally limited to tens[10,11,38] and hundreds[39–44] of gigahertz, respectively. In the present case, the lowest frequency achievable is well below 1 GHz, limited only by the time dependence of the externally applied magnetic field (Supplementary Section 14).

Coherent magnetization control in a ferrimagnet

The broad frequency content of the ultrafast magnetic field steps shown above makes them suitable for controlling magnetization in various magnetic materials that feature magnons and spin-lattice relaxation rates in the sub-gigahertz to terahertz frequency range. As a proof of principle, we apply these magnetic field steps to control the orientation of magnetization in a ferrimagnetic $Lu_{3-x}Bi_xFe_{5-y}Ga_yO_{12}$ garnet[45] (Bi:LIGG). A commercial Bi:LIGG sample with bismuth substitution $x \approx 1$ and gallium substitution $y \approx 1$ (Supplementary Section 2) was used in place of the GaP detector. The geometry of the experiment is shown in Fig. 3a. The in-plane magnetized Bi:LIGG film was ~3 µm thick and grown on a $Gd_3Ga_5O_{12}$ substrate (not shown; Supplementary Sections 2 and 3). Unlike in the measurements shown in Figs. 1 and 2, now we measure the Faraday rotation accumulated by a linearly polarized 800-nm probe pulse traversing the Bi:LIGG layer. In this configuration, the polarization rotation becomes a highly sensitive probe of the magnetization dynamics triggered in the Bi:LIGG[43,46,47]. Similar to the experiment shown in Fig. 2, a 400-nm quench pulse is used to disrupt superconductivity in the $YBa_2Cu_3O_7$ disc and trigger a magnetic field step that excites the Bi:LIGG sample.

Figure 3b shows the time-dependent changes in the *z* component of the magnetization triggered by the magnetic field step, measured

https://doi.org/10.1038/s41566-025-01651-y

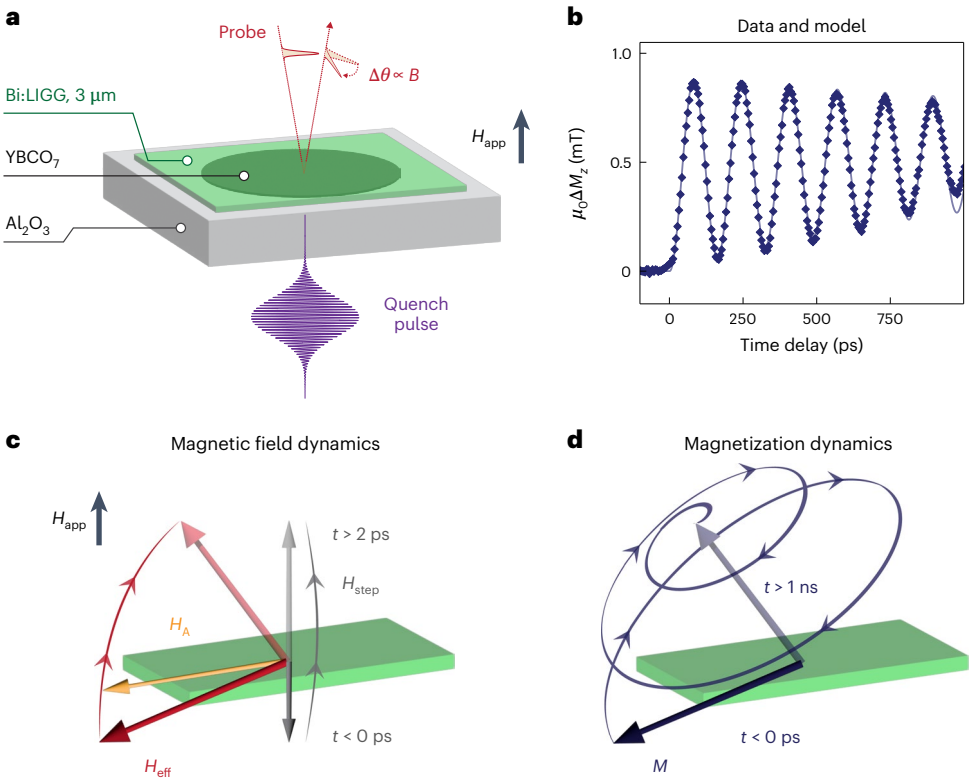

Fig. 3 | Ultrafast control of magnetization. a, Sketch of the experimental geometry. A film of Bi:LIGG is placed on top of the same $YBa_2Cu_3O_7$ disc shown in Fig. 2a. The disc is photoexcited with an ultraviolet laser pulse ($\lambda = 400$ nm) at $T = 55\ K < T_c$ to disrupt superconductivity. The magnetic field step generated (Fig. 2) triggers coherent magnon oscillations in the neighbouring Bi:LIGG sample. **b**, The data points show the time evolution of the changes in the z component of the Bi:LIGG magnetization ΔM_z, quantified by measuring the Faraday rotation above the centre of the superconducting disc versus quench-probe delay. Each data point represents the mean value ± s.e.m. (smaller than the size of the data points) extracted from a sample of 360 acquisitions (Supplementary Section 5). The fluence of the quench pulse is ~0.3 mJ cm^{-2}. At negative time delays, M_z equals −1.4 mT due to negative trapped flux before the pump pulse hits the $YBa_2Cu_3O_7$ disc (Supplementary Section 14). The solid line shows a simulation of ΔM_z above the centre of the $YBa_2Cu_3O_7$ disc using a Landau–Lifshitz–Gilbert model and the magnetic field step shown in Fig. 2b as the input bias (Supplementary Section 15). **c**, Representation of the effective magnetic field (H_{eff}) dynamics inside Bi:LIGG. H_{eff} is given by the sum of a constant field accounting for shape anisotropy (H_A) and the time-varying magnetic field step (H_{step}) generated by photoexciting the adjacent superconducting disc. H_{step} is negative at negative delays due to the trapped magnetic flux in the superconductor (Supplementary Section 14). **d**, Representation of the magnetization (M) dynamics in Bi:LIGG. Initially, M is aligned with H_{eff}. The sudden change in H_{eff} induces a precessional motion of M around the new direction of the effective field. At longer timescales, the magnetization aligns with the effective field.

in correspondence with the centre of the disc, with the same pump fluence used in Fig. 2b (~0.3 mJ cm^{-2}). As the magnetic field step excited the Bi:LIGG sample, we observed a pronounced, damped oscillation superimposed with a sudden change in magnetization direction. The frequency of the oscillations (~6 GHz) is in good agreement with the ferromagnetic resonance frequency of similar Bi-substituted rare-earth iron garnets[46,47].

Figure 3c shows a schematic of the time dependence of the magnetic field applied to the Bi:LIGG. H_{step} is the local field generated by the superconducting thin film. At negative time delays, it is antiparallel to the externally applied field H_{app} due to magnetic flux trapped in the superconductor (Supplementary Section 14). After the quench pulse hits $YBa_2Cu_3O_7$, it becomes parallel to H_{app}. H_A lies in the plane of the Bi:LIGG film to account for shape anisotropy. Due to a demagnetizing factor close to unity in our geometry[48], we set H_A equal to the saturation magnetization (~175 kA m^{-1}; see below and Supplementary Section 15). Although H_{step} varies in time, the anisotropy field H_A is constant. The combination of H_A and H_{step} gives rise to an effective magnetic field H_{eff}, along which the magnetization points in equilibrium conditions and whose changes determine the magnetization dynamics (note that the angles shown in Fig. 3c,d are exaggerated for clarity).

Figure 3d describes the dynamics of the net magnetization in Bi:LIGG. At negative pump–probe time delays, the system is in equilibrium, and the magnetization is parallel to the effective field H_{eff}. When H_{step} suddenly changes after the disruption of superconductivity in $YBa_2Cu_3O_7$, the magnetization starts precessing around the new direction of H_{eff}. The z component of the magnetization oscillates in time at a frequency given by[47,48] $\omega = \gamma(H_{step} - H_A)$, with γ representing the gyromagnetic ratio. Neglecting H_{step} (which is much smaller than the anisotropy field) and taking $\gamma/2\pi = 28$ GHz T^{-1} (ref. 49), we extract a saturation magnetization of 175 kA m^{-1} for the measured oscillation frequency of ~6 GHz (Fig. 3b). This value is in good agreement with the literature data[46] for similar Bi-substituted rare-earth iron garnets and justifies the assumptions made above. The magnetization rotation achieved is of the order of ~1° (Supplementary Section 15). For comparison, Fig. 3b (solid line) displays the result of a Landau–Lifshitz–Gilbert model calculation of the magnetization dynamics following the ultrafast magnetic field step. We set the saturation magnetization of Bi:LIGG to 175 kA m^{-1}, assume the presence of in-plane shape anisotropy only (as discussed above) and vary the damping constant to match our experimental data (Supplementary Section 15). The results of this calculation are in good agreement with the data shown in the same figure.

Discussion

The disruption of superconductivity in $YBa_2Cu_3O_7$ discs using ultraviolet laser pulses was used to perturb the magnetic field profile

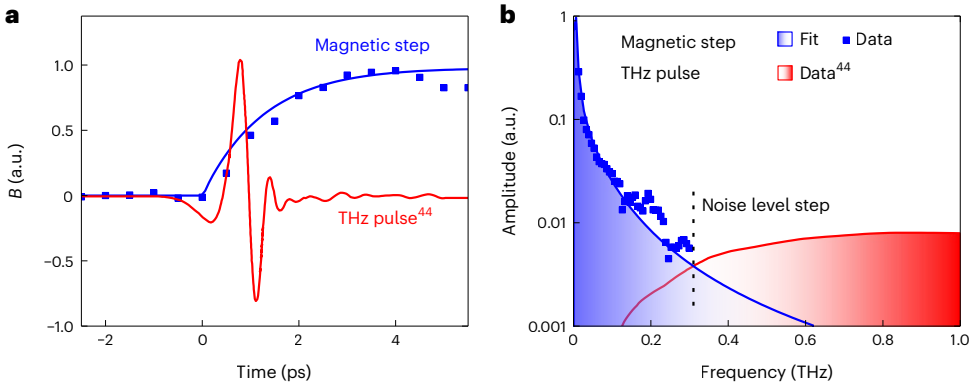

Fig. 4 | A complete set of tools for low-frequency magnetic spectroscopy. a, Experimental data (blue squares) and fit (blue solid line) for a magnetic step generated with our technique and the amplitude of the measured electric field of a single-cycle terahertz pulse[44] (red solid line). The two signals are normalized to have the same peak value. **b**, Fast Fourier transform of the time domain traces in **a**. The experimental data relative to the magnetic step (blue squares) are shown up to 0.3 THz—above which the signal falls below the noise threshold.

surrounding them and enabled the generation of magnetic field steps with ultrafast rise times and super-nanosecond-long decay times.

As shown in a proof-of-principle experiment, ultrafast magnetic field steps open up a new path towards efficient magnetization control. With the unique properties of our magnetic transient, one could switch the magnetization of a magnetic material with a coercive magnetic field of a millitesla or less. The size of our device, and therefore the region in which the ultrafast magnetic step is applied, is tailorable. For instance, faster rise times could be achieved by reducing the size of the superconducting disc down to the micrometre scale to lower the geometrical inductance of the superconducting disc (Supplementary Section 10).

We also foresee possible applications of our technique as a probing tool for quantum materials. For example, a step function with long decay times represents a suitable tool to study persistent currents in (photoexcited) superconductors. Due to its perfect conductivity, a superconductor responds to a step-like magnetic field excitation by creating superconducting currents shielding the magnetic transience for infinitely long timescales. Because our magnetic field can be switched on at timescales shorter than the lifetime of the transient state, inducing magnetic shielding currents, this time-domain technique could be used to study transient superconductors[50–54].

Furthermore, our technique can be applied as a complementary tool to terahertz time-domain spectroscopy to study low-lying excitations in a large variety of quantum materials given its broadband frequency content, ranging from sub-gigahertz to 1 THz (Fig. 4). Because the generated fields are effectively in the near field, our technique may be particularly suitable to study—using a purely magnetic excitation—samples with small lateral dimensions, inaccessible to sub-terahertz radiation. That is, for example, the case of novel two-dimensional (anti) ferromagnetic materials[55], which are available only in micrometre-scale sizes. Paired with impulsive stimulated Raman scattering, our technique could be beneficial in exploring new collective modes in these materials by enabling the estimation of the out-of-plane transient magnetization associated with low-energy spin waves.

Finally, we also envision how the amplitude of these magnetic field steps could be made larger using ultrafast demagnetization in ferromagnetic materials[56] or by quenching superconductivity in a superconductor with higher purity and first critical field. Such improvements would pave the way towards a universal tool for magnetization control.

Online content

Any methods, additional references, Nature Portfolio reporting summaries, source data, extended data, supplementary information, acknowledgements, peer review information; details of author contributions and competing interests; and statements of data and code availability are available at https://doi.org/10.1038/s41566-025-01651-y.

References

1. Back, C. H. et al. Magnetization reversal in ultrashort magnetic field pulses. *Phys. Rev. Lett.* **81**, 3251–3254 (1998).
2. Back, C. H. et al. Minimum field strength in precessional magnetization reversal. *Science* **285**, 864–867 (1999).
3. Kimel, A. V., Kalashnikova, A. M., Pogrebna, A. & Zvezdin, A. K. Fundamentals and perspectives of ultrafast photoferroic recording. *Phys. Rep.* **852**, 1–46 (2020).
4. Zalewski, T., Maziewski, A., Kimel, A. V. & Stupakiewicz, A. Ultrafast all-optical toggle writing of magnetic bits without relying on heat. *Nat. Commun.* **15**, 4451 (2024).
5. Kimel, A. V. & Li, M. Writing magnetic memory with ultrashort light pulses. *Nat. Rev. Mater.* **4**, 189–200 (2019).
6. Davies, C. S., Mentink, J. H., Kimel, A. V., Rasing, T. H. & Kirilyuk, A. Helicity-independent all-optical switching of magnetization in ferrimagnetic alloys. *J. Magn. Magn. Mater.* **563**, 169851 (2022).
7. Aradhya, S. V., Rowlands, G. E., Oh, J., Ralph, D. C. & Buhrman, R. A. Nanosecond-timescale low energy switching of in-plane magnetic tunnel junctions through dynamic Oersted-field-assisted spin Hall effect. *Nano Lett.* **16**, 5987–5992 (2016).
8. Kikuchi, N., Suyama, Y., Okamoto, S. & Kitakami, O. Pulse rise time dependence of switching field of Co/Pt multilayer dot. *Electron. Commun. Jpn* **96**, 9–14 (2013).
9. Bourne, H., Kusuda, T. & Wu, W.-H. The effect of pulse rise time on nanosecond switching in magnetic thin films. *IEEE Trans. Magn.* **6**, 391–393 (1970).
10. Wang, Z. et al. Spin dynamics triggered by subterahertz magnetic field pulses. *J. Appl. Phys.* **103**, 123905 (2008).
11. Krökel, D., Grischkowsky, D. & Ketchen, M. B. Subpicosecond electrical pulse generation using photoconductive switches with long carrier lifetimes. *Appl. Phys. Lett.* **54**, 1046–1047 (1989).
12. Stamm, C. et al. Dissipation of spin angular momentum in magnetic switching. *Phys. Rev. Lett.* **94**, 197603 (2005).
13. Tudosa, I. et al. The ultimate speed of magnetic switching in granular recording media. *Nature* **428**, 831–833 (2004).
14. van der Ziel, J. P., Pershan, P. S. & Malmstrom, L. D. Optically-induced magnetization resulting from the inverse Faraday effect. *Phys. Rev. Lett.* **15**, 190–193 (1965).
15. Ju, G. et al. Ultrafast nonequilibrium spin dynamics in a ferromagnetic thin film. *Phys. Rev. B* **57**, R700–R703 (1998).
16. Kimel, A. V. et al. Ultrafast non-thermal control of magnetization by instantaneous photomagnetic pulses. *Nature* **435**, 655–657 (2005).

17. Satoh, T. et al. Spin oscillations in antiferromagnetic NiO triggered by circularly polarized light. *Phys. Rev. Lett.* **105**, 077402 (2010).
18. Nova, T. F. et al. An effective magnetic field from optically driven phonons. *Nat. Phys.* **13**, 132–136 (2017).
19. Basini, M. et al. Terahertz electric-field-driven dynamical multiferroicity in $SrTiO_3$. *Nature* **628**, 534–539 (2024).
20. Juraschek, D. M. & Spaldin, N. A. Orbital magnetic moments of phonons. *Phys. Rev. Mater.* **3**, 064405 (2019).
21. Merlin, R. Unraveling the effect of circularly polarized light on reciprocal media: breaking time reversal symmetry with non-Maxwellian magnetic-esque fields. *Phys. Rev. B* **110**, 094312 (2024).
22. Tinkham, M. *Introduction to Superconductivity* (Courier Corporation, 2004).
23. Poole, C. P., Farach, H. A., Creswick, R. J & Prozorov, R. *Superconductivity* (Elsevier, 2014).
24. Kaindl, R. A., Carnahan, M. A., Chemla, D. S., Oh, S. & Eckstein, J. N. Dynamics of Cooper pair formation in $Bi_2Sr_2CaCu_2O_{8+\delta}$. *Phys. Rev. B* **72**, 060510 (2005).
25. Pashkin, A. et al. Femtosecond response of quasiparticles and phonons in superconducting $YBa_2Cu_3O_{7-\delta}$ studied by wideband terahertz spectroscopy. *Phys. Rev. Lett.* **105**, 067001 (2010).
26. Demsar, J. Non-equilibrium phenomena in superconductors probed by femtosecond time-domain spectroscopy. *J. Low Temp. Phys.* **201**, 676–709 (2020).
27. Averitt, R. D. et al. Nonequilibrium superconductivity and quasiparticle dynamics in $YBa_2Cu_3O_{7-\delta}$. *Phys. Rev. B* **63**, 140502 (2001).
28. Demsar, J. et al. Pair-breaking and superconducting state recovery dynamics in MgB_2. *Phys. Rev. Lett.* **91**, 267002 (2003).
29. Kaindl, R. A. et al. Ultrafast mid-infrared response of $YBa_2Cu_3O_{7-\delta}$. *Science* **287**, 470–473 (2000).
30. Polyanskii, A. A. & Larbalestier, D. C. in *Handbook of Superconductivity* 371–382 (CRC Press, 2021).
31. Riordan, J. A. & Zhang, X.-C. Sampling of free-space magnetic pulses. *Opt. Quantum Electron.* **32**, 489–502 (2000).
32. Fava, S. et al. Magnetic field expulsion in optically driven $YBa_2Cu_3O_{6.48}$. *Nature* **632**, 75–80 (2024).
33. Yuan, Y., Theile, J. & Engemann, J. Measurement of the Meissner effect by a magneto-optic a.c. method using ferrimagnetic garnet films. *J. Magn. Magn. Mater.* **95**, 58–60 (1991).
34. Koblischka, M. R. & Wijngaarden, R. J. Magneto-optical investigations of superconductors. *Supercond. Sci. Technol.* **8**, 199 (1995).
35. Freeman, M. R. Picosecond studies of nonequilibrium flux dynamics in superconductors. *MRS Online Proc. Libr.* **290**, 323 (1992).
36. Krupka, J. et al. Complex conductivity of YBCO films in normal and superconducting states probed by microwave measurements. *IEEE Trans. Appl. Supercond.* **23**, 1501011 (2013).
37. Winzer, K. & Kumm, G. Fluctuation-enhanced conductivity and magnetoconductivity of high-quality $YBa_2Cu_3O_{7-\delta}$ crystals. *Z. Physik. B* **82**, 317–321 (1991).
38. Auston, D. H. Picosecond optoelectronic switching and gating in silicon. *Appl. Phys. Lett.* **26**, 101–103 (1975).
39. Song, H.-J. & Nagatsuma, T. (eds) *Handbook of Terahertz Technologies: Devices and Applications* (Jenny Stanford, 2015).
40. Blank, T. G. H. et al. Effective rectification of THz electromagnetic fields in a ferrimagnetic iron garnet. *Phys. Rev. B* **108**, 094439 (2023).
41. Hirori, H., Doi, A., Blanchard, F. & Tanaka, K. Single-cycle terahertz pulses with amplitudes exceeding 1 MV/cm generated by optical rectification in $LiNbO_3$. *Appl. Phys. Lett.* **98**, 091106 (2011).
42. Hebling, J., Almási, G., Kozma, I. Z. & Kuhl, J. Velocity matching by pulse front tilting for large-area THz-pulse generation. *Opt. Express* **10**, 1161–1166 (2002).
43. Mashkovich, E. A. et al. Terahertz-driven magnetization dynamics of bismuth-substituted yttrium iron-gallium garnet thin film near a compensation point. *Phys. Rev. B* **106**, 184425 (2022).
44. Yeh, K.-L., Hebling, J., Hoffmann, M. C. & Nelson, K. A. Generation of high average power 1 kHz shaped THz pulses via optical rectification. *Opt. Commun.* **281**, 3567–3570 (2008).
45. Hansteen, F. et al. Optical and magnetooptical properties of bismuth and gallium substituted iron garnet films. *Thin Solid Films* **455–456**, 429–432 (2004).
46. Hansen, P., Witter, K. & Tolksdorf, W. Magnetic and magneto-optic properties of lead- and bismuth-substituted yttrium iron garnet films. *Phys. Rev. B* **27**, 6608–6625 (1983).
47. Deb, M. et al. Picosecond acoustic-excitation-driven ultrafast magnetization dynamics in dielectric Bi-substituted yttrium iron garnet. *Phys. Rev. B* **98**, 174407 (2018).
48. Kittel, C. *Introduction to Solid State Physics* 8th edn (Wiley, 2018).
49. Will-Cole, A. R. et al. Negligible magnetic losses at low temperatures in liquid phase epitaxy grown $Y_3Fe_5O_{12}$ films. *Phys. Rev. Mater.* **7**, 054411 (2023).
50. Fausti, D. et al. Light-induced superconductivity in a stripe-ordered cuprate. *Science* **331**, 189–191 (2011).
51. Kaiser, S. et al. Optically induced coherent transport far above T_c in underdoped $YBa_2Cu_3O_{6+\delta}$. *Phys. Rev. B* **89**, 184516 (2014).
52. Nicoletti, D. et al. Optically induced superconductivity in striped $La_{2-x}Ba_xCuO_4$ by polarization-selective excitation in the near infrared. *Phys. Rev. B* **90**, 100503 (2014).
53. Mitrano, M. et al. Possible light-induced superconductivity in K_3C_{60} at high temperature. *Nature* **530**, 461–464 (2016).
54. Isoyama, K. et al. Light-induced enhancement of superconductivity in iron-based superconductor $FeSe_{0.5}Te_{0.5}$. *Commun. Phys.* **4**, 160 (2021).
55. Mak, K. F., Shan, J. & Ralph, D. C. Probing and controlling magnetic states in 2D layered magnetic materials. *Nat. Rev. Phys* **1**, 646–661 (2019).
56. Beaurepaire, E., Merle, J.-C., Daunois, A. & Bigot, J.-Y. Ultrafast spin dynamics in ferromagnetic nickel. *Phys. Rev. Lett.* **76**, 4250–4253 (1996).

Methods
All methods can be found in the Supplementary Information.

Data availability
Source data are provided with this paper. All other data that support the plots within this paper and other findings of this study are available from the corresponding authors on request.

Acknowledgements
We acknowledge support from the Deutsche Forschungsgemeinschaft (DFG) by the Cluster of Excellence CUI: Advancing Imaging of Matter (EXC 2056, project ID 390715994) to G.D.V., G.J. and A.C. We thank M. Volkmann, I. Khayr and P. Licht for their technical assistance. We are also grateful to B. Fiedler, B. Höhling and T. Matsuyama for their support in the fabrication of electronic devices used on the measurement setup and to E. König, L. Navratilova, G. Meier and D. Nicoletti for help with the sample fabrication and characterization.

Author contributions
A.C., G.J. and M.B. conceived the experiment. A.C. supervised the project. The experimental setup was built by G.D.V., G.J. and T.G., and the related measurements were performed by G.D.V. and M.B. Data analysis was performed by G.D.V., S.F., G.J. and M.B. Theoretical simulations were performed by G.D.V., M.F. and M.B. The manuscript was written by G.D.V., S.F., M.B., G.J., A.V.K. and A.C. with contributions from all co-authors.

Funding
Open access funding provided by Max Planck Society.

Competing interests
The authors declare no competing interests.

Additional information
Supplementary information The online version contains supplementary material available at https://doi.org/10.1038/s41566-025-01651-y.

Correspondence and requests for materials should be addressed to G. Jotzu, M. Buzzi or A. Cavalleri.

Peer review information *Nature Photonics* thanks the anonymous reviewers for their contribution to the peer review of this work.